Available online at www.sciencedirect.com
ScienceDirect
Journal of the European Ceramic Society 28 (2008) 2487–2494
www.elsevier.com/locate/jeurceramsoc

Microstructural and morphological analysis of nanostructured alumina particles synthesized at low temperature via aerosol route

M.I. Martín [a,*], M.E. Rabanal [a], L.S. Gómez [a], J.M. Torralba [a], O. Milosevic [b]

[a] *University Carlos III de Madrid, Avda. de la Universidad 30, 28911 Leganés, Madrid, Spain*
[b] *Institute of Technical Sciences of Serbian Academy of Sciences and Arts, K. Mihailova 35/IV, 11000 Belgrade, Serbia*

Received 27 July 2007; received in revised form 11 March 2008; accepted 15 March 2008
Available online 21 May 2008

Abstract

Nanometer-sized particles (1–100 nm) are of considerable interest for a wide variety of applications, ranking from catalyst to luminescence ceramics, due to their unique and improved properties primarily determined by size, composition and structure. In this study, we report a simple, rapid aerosol decomposition process for the continuous synthesis of nanoparticles with adjustable sizes, narrow size distribution, high crystallinity and good stoichiometry.

This paper presents the preparation and characterization of nanostructured spherical alumina particles (<500 nm sized) by low temperature aerosol synthesis for the application in MMCs reinforcement. Synthesis procedure includes aerosol formation ultrasonically from alumina nitrate water solution and its decomposition into a tubular flow reactor at 400 °C. Consequently, as-obtained particles are spherical, smooth, amorphous and in non-agglomerated state. The phase crystallization, either into γ-Al_2O_3 or α-Al_2O_3 is promoted by additional thermal treatment ranging between 700 °C and 1300 °C. Detailed phase and structural analyses were carried out using X-ray powder diffraction (XRD), scanning electron microscopy (SEM/EDS) and analytical and high-resolution transmission electron microscopy (TEM/HRTEM).

Keywords: Nanoparticles; Spray Pyrolysis; Al_2O_3; Aerosols

1. Introduction

A particular interest in ultrafine particles or nanoparticles (ranging between a few nanometers and 100 nm) lies in the fact that they may be remarkably different from those in the bulk form in terms of chemical and physical behaviour. They hold great potential for use in electronic, chemical or mechanical industries, as well as in relevant technologies, including superconductors, catalysts, magnetic materials, pigments, structural and engineering materials.

Aluminium oxide nanoparticles have important applications in ceramic industry[1,2] and can be used as an abrasive material, in heterogeneous catalysis, as an absorbent, a biomaterial and as reinforcements of metal–matrix composites (MMCs).[3–5] Metal–matrix composites (MMCs) having fine-scale and uniformly dispersed phases, are of great technological interest because of improved mechanical properties, particularly the hardness, wear resistance, elastic modulus and yield strength. The addition of ceramic alumina nanoparticles into metal–matrix composites might have considerable implications for their application in automotive, defense and aerospace industries.

In order to be used for effective discontinuous reinforcements in a continuous metal–matrix, Al_2O_3 particles have to fulfill certain structural and morphological requirements: small particle size and narrow size distribution, large surface area, spherical morphology and the absence of agglomerates. As far as the hot wall aerosol synthesis method (Spray Pyrolysis), as basically chemical route for obtaining advanced materials, is concerned, it offers several advantages in the preparation of well-defined oxide powders over conventional synthesis.[6]

The Spray Pyrolysis technique is based on ultrasonic generation of micrometric-sized aerosol droplets and their decomposition at intermediate temperatures (400–800 °C). Due to precipitation, decomposition and chemical reaction occur in a dispersed phase and in a single step, allowing control of

* Corresponding author. Tel.: +34 916249482; fax: +34 916249430.
E-mail address: mariaisabel.martin@uc3m.es (M.I. Martín).

0955-2219/$ – see front matter © 2008 Elsevier Ltd. All rights reserved.
doi:10.1016/j.jeurceramsoc.2008.03.019

Nomenclature

Nomenclature

c	mass concentration of the precursor solution (10^{-3} kg m^{-3})
D_o	the droplet mean size (μm)
D_p	the particle mean size (μm)
f	the ultrasound frequency (10^{-6} s^{-1})
M_{oxide}	molecular mass of the resulting compound (g mol^{-1})
M_{prec}	molecular mass of precursor salt (g mol^{-1})
γ	the liquid (solution) surface tension (10^{-3} N m^{-1})
ρ	the liquid (solution) density (10^{-3} kg m^{-3})

important particle properties (size, morphology, chemical composition, etc.) simply by controlling the process parameters (residence time, decomposition temperature).[7–12]

This paper describes the low temperature aerosol synthesis (LTAS) and structural and morphological characterization of nanostructured alumina particles for the application in metal–matrix composites for nanoreinforcements. The low temperature aerosol synthesis was chosen in order to synthesize the amorphous powder without the onset of crystallization and to promote and control the crystallization via additional thermal treatment. Aluminium nitrate nonahydrate was chosen as precursor because of its low temperature thermal decomposition (up to 400 °C) accompanied with melting of crystallo-hydrates, dehydration and elimination of nitrogen compounds followed by powder amorphization within a relatively narrow temperature range.[13] For that purpose, the conditions for the production of high-purity nanoparticles, spherical and aggregate-free, will be optimized by establishing a correlation between the processing parameters (ultrasound frequency, decomposition temperature, residence time, solution properties) and the morphology and structural properties of the nanopowders.

2. Experimental procedure

2.1. Particle synthesis

The Spray Pyrolysis experimental set-up consists of an ultrasonic nebulizer (RBI), a quartz tube located inside a cylindrical furnace (LENTON, l–0.95 m) and a water collector (Fig. 1). An aqueous precursor solution was prepared by dissolving the corresponding amount of aluminium nitrate nonahydrate ($Al(NO_3)_3{\cdot}9H_2O$, p.a., 99.997% purity, Aldrich) in order to obtain 0.1×10^3 mol m^{-3} (0.0375×10^3 kg m^{-3}) concentration. The initial solution was atomized using an ultrasonic vibrating frequency of 2.1×10^6 s^{-1}. The aerosol was transported into a reaction zone and decomposed at 400 °C. Air was used as a carrier gas. Its flow rate was 2.5×10^{-5} m^3 s^{-1}, whereas the droplet/particle residence time, calculated from the carrier gas flow rate and the geometry of the reactor, was 18.6 s. The particles were water collected at exhaust.

The mean droplet sizes of generated aerosol droplets were estimated in accordance to the following Lang's equation[14] (notation for the symbols is given in Nomenclature):

$$D_o = 0.34\left(\frac{8\pi\gamma}{\rho f^2}\right)^{0.33} \quad (1)$$

The predicted particle size, D_p, can be expressed as a function of the droplet size, D_o, in accordance with the following relation[15]:

$$D_p = \left(\frac{M_{oxide}}{M_{prec.}}\frac{c}{\rho}\right)^{0.33} D_o \quad (2)$$

The values estimated were as follows: $D_o = 2.74$ μm, $D_p = 0.37$ μm (375 nm).

After synthesis, the powders were isothermally annealed in air at 700–1300 °C for 12 h (chamber furnace CHESA) to promote phase crystallization.

The physicochemical properties of the precursor solutions were carefully controlled and monitored as follows: pH 2.56 (Orion research pH/milivoltmetar 611); density, $\rho = 1.01493 \times 10^{-3}$ kg m^{-3} (AP-PAAR density meter DMA 55), surface tension, $\sigma = 64.4 \times 10^{-3}$ N m^{-1} (Digital K10T Kruss tensiometer) and viscosity, $\nu = 1.064315758 \times 10^{-3}$ Pa (MLW Viscosimeter B3). Measurements were made at room temperature.

2.2. Particle characterization

Thermal analysis of the "*as-prepared*" and annealed powder samples was performed using thermogravimetry in air on a PerkinElmer, Pyris 1 TGA instrument with a heating rate of 10 °C min^{-1}.

The crystal structure of the "*as-prepared*" and thermally treated powders was analyzed by X-ray powder diffraction (XRD) in combination with electron diffraction–high-resolution transmission electron microscopy (HRTEM). An automatic X' Pert Philips diffractometer, using a CuKα source (λ = 1.5418 Å), in the 10–70° 2θ range in the step-scanning mode with a step size of 0.04° was used. Crystalline phases were identified and indexed by means of X-Ray Diffraction Philips Analytical[16] software and the Pcpdfwin database—JCPDS-ICDD.[17] Electron diffraction and HRTEM were interpreted using Electron Diffraction Pattern Simulations for Windows and Digital Micrograph programs.[18]

Chemical composition, homogeneity and particle morphology were examined by scanning electron microscopy (SEM) equipped with energy dispersive X-ray analysis (EDAX) on a Philips XL 30 and transmission electron microscopy (TEM, JEOL-JEM, 400 kV). Prior to SEM analysis, the particles were ultrasonically disagglomerated for 10 min in an ultrasonic bath, disposed onto aluminium substrate and sputtered with gold. TEM samples were prepared by ultrasonic dispersion of a small portion of powder in acetone; this suspension was further placed on a 3-mm carbon coated copper grid. Primary nanoparticles were identified using the JEOL JEM 4000EX, operated at 400 kV with a resolution of 1.8 Å (point to point).

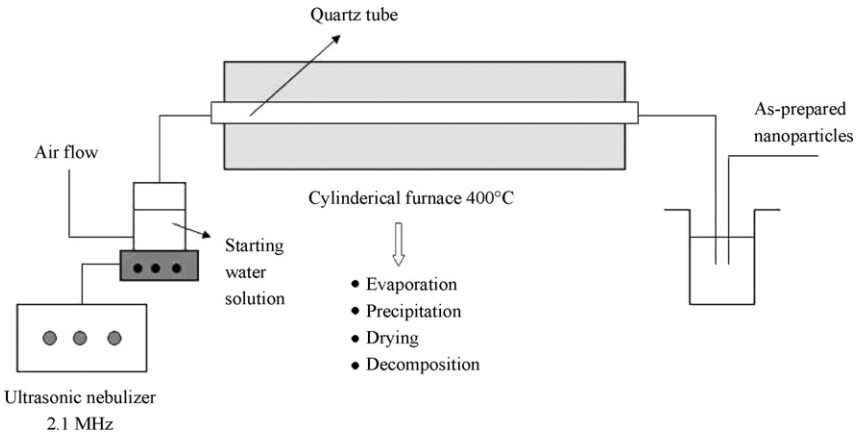

Fig. 1. Schematic representation of the processing equipment.

Digital images were processed using digital Micrograph™ software package. Measurements were carried out using pixel scale (1 pixel: 0.625 nm × 0.625 nm, in this case 1 nm = 1.6 pixels). Primary particles were identified as individual particles with different contrasts and visually perceptible contour features. Measurements of the D_{max} were carried out manually.

3. Results and discussion

Fig. 2a shows X-ray diffraction patterns for the "*as-prepared*" and thermally treated (≤800 °C) powder samples. In both cases, the amorphous character is typically reflected in the shape of the patterns. However, after a thermal treatment at 900 °C/12 h, a change in the amorphous behaviour can be perceived, manifesting itself through low-intensity reflections corresponding to the γ-Al_2O_3 phase with cell parameter of $a = 7.924$ Å (JCPDS 10-0425, S.G. 227), where the (4 0 0) and the (4 4 0) peaks at 2θ 45.8° and 67°, respectively, can be identified too. By increasing the temperature, the maximum related to the γ phase appears, though the shape of the diffractogram is still broad. Other polymorphs associated with γ-Al_2O_3 could be present in very small quantities in the samples treated at 1000 °C and 1100 °C. They correspond to the main peaks of a δ-Al_2O_3 (JCPDS = 16-0394, $a = 7.943$ Å, $c = 23.5$ Å) having the strongest lines at 1.39 nm (2θ = 66°), 1.98 nm (2θ = 45.6°) and 2.4 nm (2θ = 36.4°). There is also evidence of the χ-Al_2O_3 phase (JCPDS = 13-0373 Å, $a = 5.57$ Å, $c = 8.64$ Å), with the strongest peaks at 1.39 nm (2θ = 67°), 2.41 nm (2θ = 37.2°) and 2.12 nm (2θ = 42.6°). At 1200 °C, the appearance of an intermediate phase δ-Al_2O_3 is obviously coexistent with the γ-Al_2O_3 phase, although, some low-intensity peaks at approximately 2θ = 43°, 57.4° and a peak over 35°, corresponding to (1 1 3), (1 1 6) and (1 0 4) reflections indicate the emergence of the α-Al_2O_3 phase (JCPDS 42-1468, S.G. = 167, $a = 4.758$ Å, $c = 12.99$ Å). After 1300°/12 h annealing, only well-defined peaks of α-Al_2O_3 phase can be noticed. Apart from the main phases encountered in the sample, small peaks corresponding to the SiO_2 residues of the reactor quartz tube, can also be detected.

The thermal decomposition of the "*as-prepared*" and thermally treated powder samples is presented in Fig. 2b. The decomposition curve of the "*as-prepared*" powders indicates that decomposition is not fully achieved with the overall mass loss of about 70.7% at 510 °C. Since the process of aluminium nitrate nonahydrate decomposition occurs at temperatures below

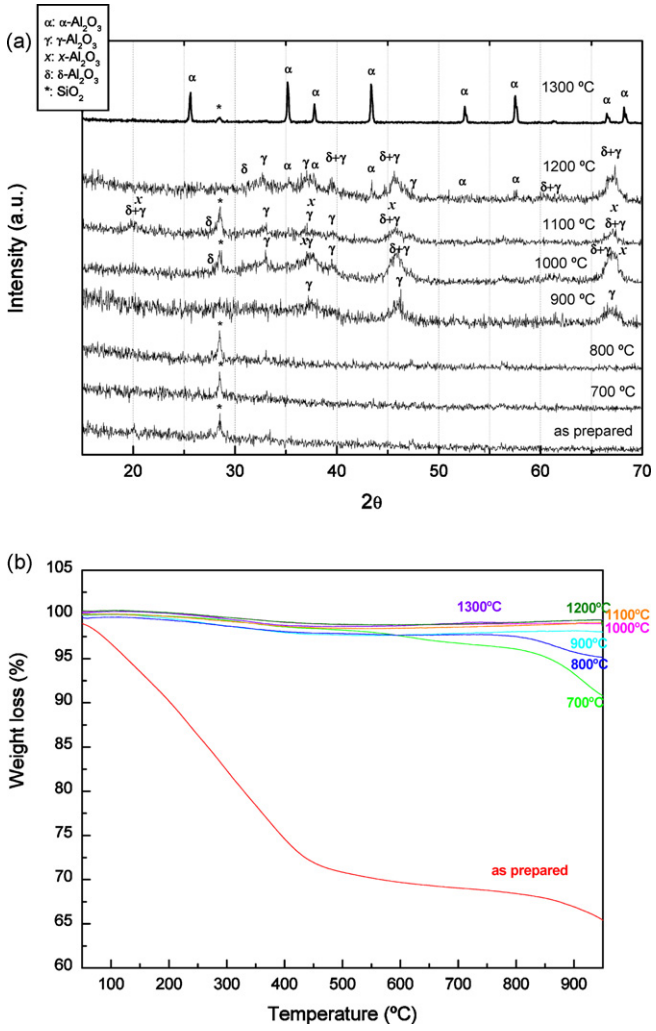

Fig. 2. (a) Experimental X-ray diffraction patterns for "*as-prepared*" and thermally treatment powder samples. (b) TG curves for the "*as-prepared*" and thermally treated powders samples.

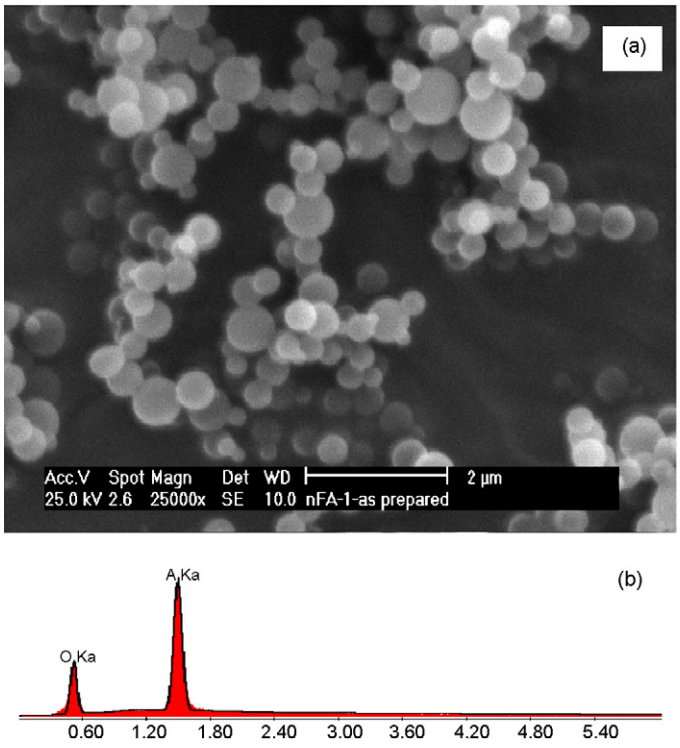

Fig. 3. SEM micrograph of "*as-prepared*" Al_2O_3 particles (a) and the corresponding EDS analysis (b).

500 °C through simultaneous reactions of dehydration, hydrolysis and destruction of the nitrate group[13] preceded by salt melting at 80 °C, the observed decomposition behaviour is presumably caused by high heating rates and short residence time in the high temperature zone during aerosol synthesis. However, additional thermal treatment resulted in complete powder decomposition.

Fig. 3a shows SEM micrographs of the "*as-prepared*" Al_2O_3 particles. It can be noticed that the "*as-prepared*" particles obtained by aerosol decomposition are highly spherical, smooth, non-aggregated and relatively uniform in size (below 500 nm). EDAX analyses (Fig. 3b) confirm high compositional uniformity and the exclusive presence of the constitutive elements.

Fig. 4 corresponds to SEM images taken with secondary electron mode detector for thermally treated powder samples at 700–1200 °C during a 12-h period. It is evident that particle morphology does not change significantly with annealing. Powders persist in their unagglomerated form, although high temperature regime brings about further crystallization and the growth of primary particles.[6] Thermal treatment at 1300 °C/12 h does not result in significant change in particle morphology, which is illustrated in Fig. 5, showing spherical and mostly non-aggregated particles, although there are indications of particle bonding and neck formation.

Low magnifications in bright field mode allowed the identification the structure and growth of primary nanoparticles aroused through the collision/coalescence mechanisms. Fig. 6 shows a low magnification TEM image in bright field mode of a secondary particle, 250 nm in diameter, annealed at 1100 °C/12 h. Further magnification and contrast analysis reveal small subspheric primary nanoparticles with D_{max} 13.6 ± 3 nm. The contrast at the external edge of the particles suggests the presence of approximately 8–8.5 nm thick crust at the particle surface. The primary particles are in mutual contact indicating collision and initial stages of sintering process. The amorphous and polycrystalline character of the particles, typical for the "*as-prepared*" and low temperature thermally treated samples, did not allow the

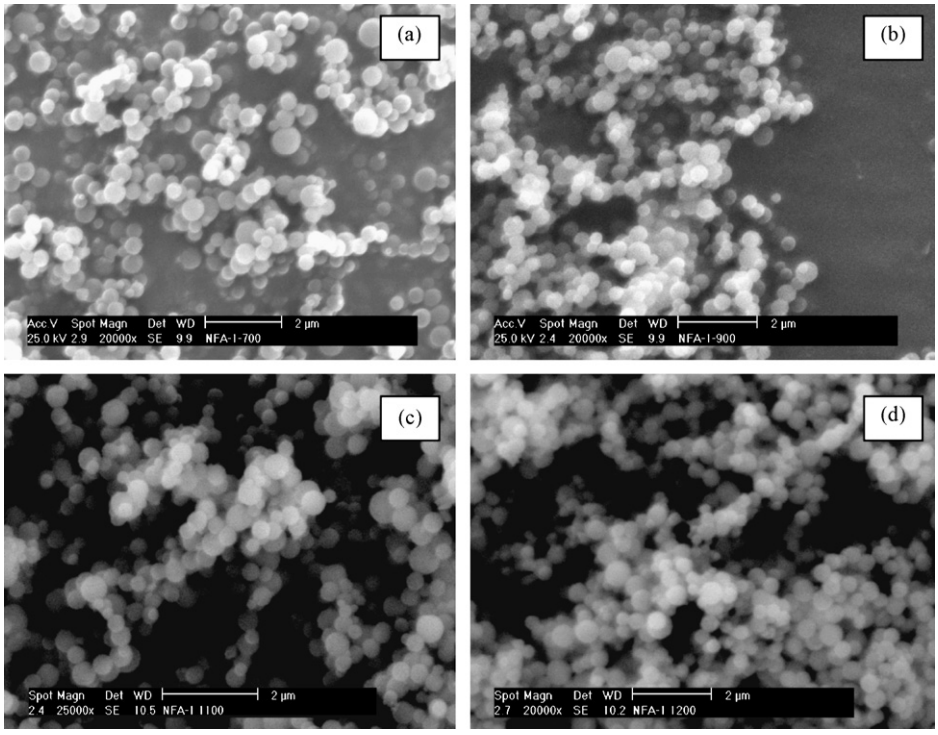

Fig. 4. SEM micrographs of the thermally treated powder samples: (a) 700 °C/12 h, (b) 800 °C/12 h, (c) 1100 °C/12 h, (d) 1200 °C/12 h.

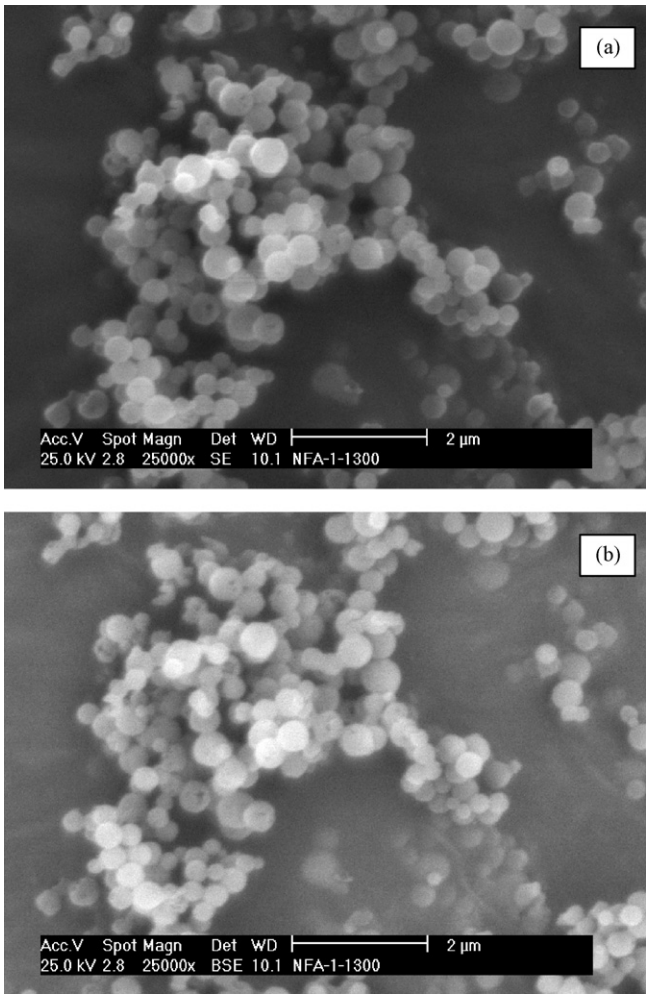

Fig. 5. SEM micrograph of sample annealed at 1300 °C/12 h: (a) secondary electrons (SE), (b) backscattered electrons (BSE).

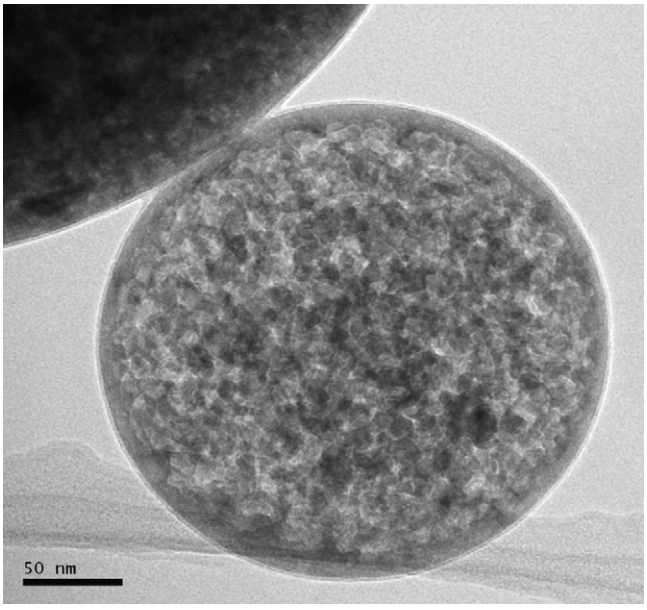

Fig. 6. Low resolution image TEM in bright field mode for Al_2O_3 after a thermal treatment at 1100 °C/12 h.

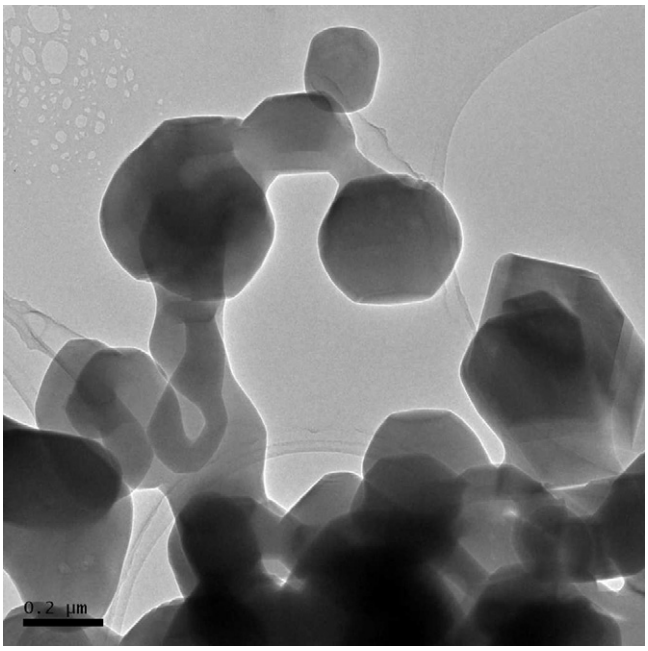

Fig. 7. Low resolution image TEM in bright field mode for Al_2O_3 after a thermal treatment at 1300 °C/12 h.

acquisition of high-quality HRTEM images. Quite oppositely, thermal treatment at 1300 °C/12 h provokes the bonding of secondary particles and sintering, followed by neck formation, as evident in the low magnification TEM image (Fig. 7).

Fig. 8 shows a selected area electron diffraction pattern (SAEDP) taken from the sample annealed at 1100 °C/12 h indexed in accordance to the γ-Al_2O_3 phase (JCPDS = 29-0063), having a defect spinel structure.[19,20] Table 1 represents the

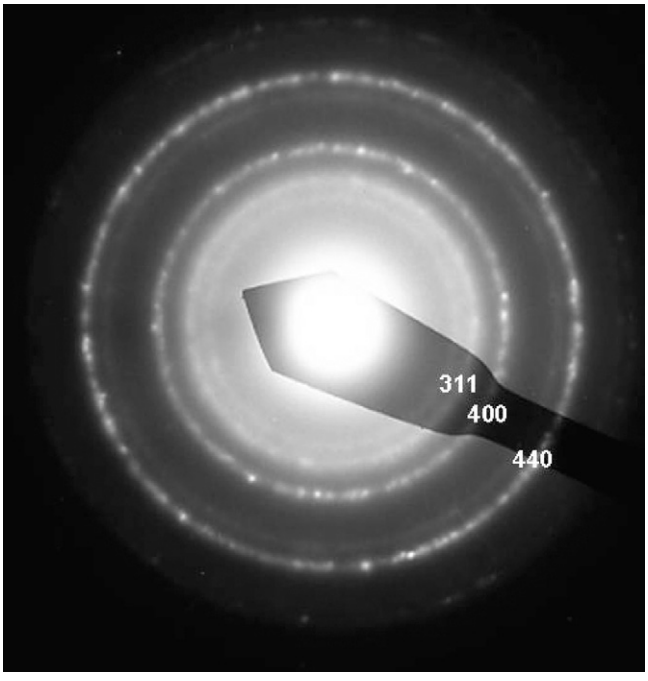

Fig. 8. SAEDP of the sample annealed at 1100 °C/12 h indexed according to the γ-Al_2O_3 phase.

Table 1
Comparison between d-spacings for the γ-Al_2O_3 phase and η-Al_2O_3 phases according to Lippens and de Boer[21] and the distances obtained in this study

γ-Al_2O_3[a] (Å)	η-Al_2O_3[a] (Å)	This paper (Å)	*h k l*	Intensity
4.6	4.57	4.642	1 1 1	Diffuse
2.77	2.76	2.722	2 2 0	Weak
2.39	2.395	2.394	3 1 1	Strong
2.284	2.284	2.285	2 2 2	Weak
1.99	1.98	1.998	4 0 0	Strong
1.956	–	1.947	4 0 0	Strong
1.52	1.519	1.527	5 1 1/3 3 3	Weak
1.407	1.396	1.418	4 4 0	Strongest
1.395	–	1.397	4 4 0	Strongest

[a] After Lippens B.C. and de Boer J.H.[21]

Table 2
Comparison between d-spacings for the α-Al_2O_3 phase according to Welton-Holzer J., McCarthy G. (JCPDS 42-1463) and the distances obtained in this study

(α-Al_2O_3)[a] (Å)	This paper (Å)	*h k l*	Intensity
	3.881	1 0–1 1	Weak
3.48	3.460	0 1–1 2	Very strong
2.085	2.071	1 1–2 3	Strongest
1.964	1.910	2 0–2 2	Weak
1.404	1.401	2 1–3 4	Strong
1.336	1.331	1 2–3 5	Weak

[a] Welton-Holzer J., McCarthy G.[22]

d-spacing comparison between the γ-Al_2O_3 and η-Al_2O_3 phases obtained in this study via selected area electron diffraction patterns (SAEDP) and the corresponding literature values.[21] Although, the γ-Al_2O_3 and η-Al_2O_3 phases are pretty similar, slight differences in the (4 0 0) and (4 4 0), typical for the γ-Al_2O_3 phase, allow to assume that the results obtained in this paper closely approximate the γ-Al_2O_3 phase proposed by Lippens and de Boer.[21] Fig. 9 corresponds to the SAEDP obtained for the sample annealed at 1300 °C. The maximum is indexed based on a rhombohedral R-3c structure (1 6 7) typical of the α-Al_2O_3 phase. Table 2 represents the d-spacings for the α-Al_2O_3 phase indicating a good agreement between the obtained and relevant literature values (according to Welton-Holzer J., McCarthy G. (JCPDS 42-1463)).[22]

HR-TEM confirmed the presence of α-Al_2O_3 phase in the powder samples treated at 1300 °C/12 h (Fig. 10). Based on the high-resolution transmission electron microscopy technique in bright field mode, the main plane (1 0 4) along the [0 0 1] zone axis can be resolved and as inset the *fft* (fast fourier transformed) confirms the trigonal symmetry (S.G. R-3c). Moreover, a better order related to the orientation of atomic frames and the decreased occurrence of defects coinciding with the rhombohedral α-Al_2O_3 phase marked by well-defined corundum structure are evident.

The existence of several Al_2O_3 structures during the γ-to-α-Al_2O_3 phase transformation, including the typical γ-Al_2O_3 and α-Al_2O_3, have been reported by several authors.[11,19–25] As previously mentioned by Levin and Brandon,[27] the metastable Al_2O_3 structures can be divided into two broad categories: a face centered cubic (fcc) or a hexagonal close packed (hcp) arrangement of oxygen anions. Based on the fcc packing, the γ (cubic), η (cubic), θ (monoclinic) and δ (tetragonal or orthorhombic) phases can be established, whereas based on hcp packing, the α (trigonal), κ (orthorhombic), χ (hexagonal) phases have been identified. The most complete study has been carried out by Levin et al.[26] and Wefer and Misra,[28] in which they identified the alumina transitions corresponding to different temperature

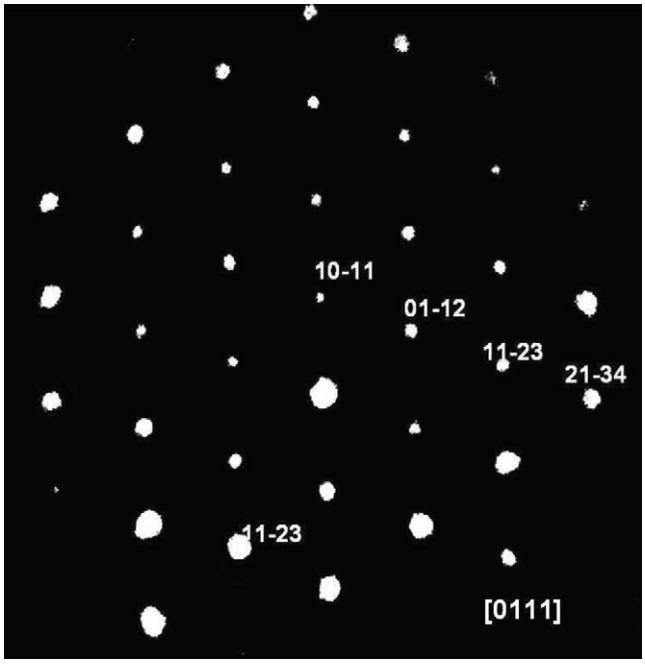

Fig. 9. SAEDP of the sample annealed at 1300 °C/12 h, along the [0 1 1 1] zone axis indexed according to the α-Al_2O_3 phase.

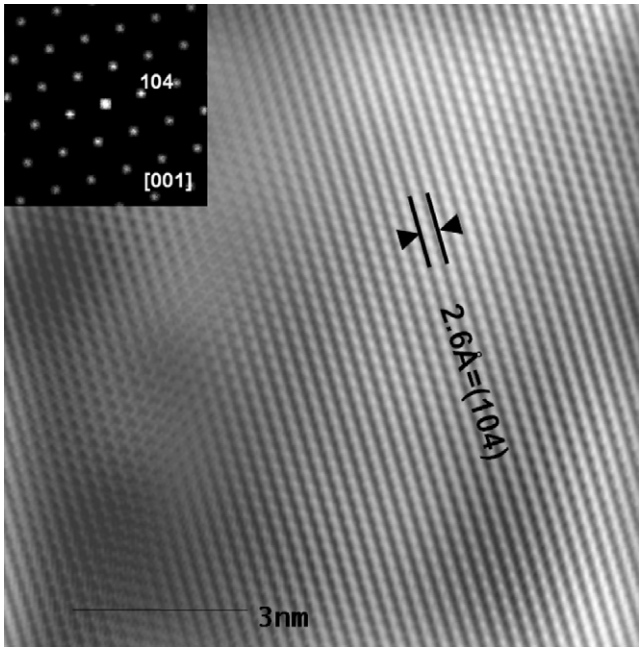

Fig. 10. Filtered HRTEM image in bright field mode of a sample post treated at 1300 °C/12 h. In the left corner (as inset) is shown the *fft* along the [0 0 1] zone axis.

ranges of stability, derived from partially dehydrated aluminium hydroxides.

Vallet-Regí et al.[11] have synthesized alumina using Spray Pyrolysis method, confirming the γ-Al_2O_3 phase at 400 °C, γ → α transition at 1100 °C, and the α-Al_2O_3 phase at 1200 °C. The same authors proved the presence of the θ-Al_2O_3 phase in addition to γ-Al_2O_3 by changing the pyrolysis temperature to 900 °C. Webster et al.[29] have identified the following phases in the development of nanosized Al_2O_3 fibres: the γ-Al_2O_3 phase, the γ + δ-Al_2O_3 phase, the θ + δ-Al_2O_3 phase and α-Al_2O_3 by sintering at 600 °C, 800 °C, 1000 °C and 1200 °C, respectively. However, in the case of flame Spray Pyrolysis, only the presence of the γ- and α-Al_2O_3 phases[24] was confirmed. Furthermore, the synthesis in air atmosphere seems to favour the formation of the δ-Al_2O_3 phase and the κ-Al_2O_3 phase in fine materials as reported by several authors.[27,28] Therefore, as established by Paglia,[19] Peter Østbo,[23] and Levin and Brandon[27] there still exists considerable controversy over the definitive structures of many of the alumina phases.

In this paper, the XRD results suggest the presence of both δ-Al_2O_3 and χ-Al_2O_3 phases, as intermediate phases during the γ-to-α-Al_2O_3 phase transformation.

The θ (monoclinic) or δ (tetragonal or orthorhombic) phases has been reported as metastable crystalline phases formed by rapid quenching from the melt, vapour deposition or crystallization of amorphous alumina, or formed during the heating of amorphous alumina films by anodization.[21] Other polymorphs could be also present in the samples in very small quantities; however the XRD resolution associated with the amorphous and nanocrystalline particle structure, does not allow to identify them either by XRD or HRTEM. However, it might be possible that these phases contribute in XRD peaks broadening.

4. Conclusions

The paper presents the LTAS of fine Al_2O_3 particles (<500 nm) followed by XRPD and electron microscopy characterization. The "*as-prepared*" particles and samples treated at temperatures up to 800 °C are amorphous. XRPD and electron diffraction-HRTEM show the presence of two polycrystalline phases after the high temperature treatment: γ and α, the latter prevailing at 1300 °C/12 h. Microscopic observations indicate that obtained Al_2O_3 particles are spherical, smooth and non-agglomerated. High temperature (700–1300 °C) annealing did not have significant impact on the particle morphology. Owing to well-controlled and well-defined properties, these particles could presumably be applied as discontinuous reinforcement for MMCs.

Acknowledgments

The authors gratefully appreciate the financial support of the Ministry for Education and Science of Spain, Juan de la Cierva Program JCI-2005-1892-13 (M.I. Martín), MAT2006-02458 project and Sabatic Grant SAB 2004-0035 (O. Milosevic). The assistance in TEM characterization of the Electron Microscopy and Citometry Center, University Complutense, Madrid, Spain is also kindly acknowledged.

References

1. Zieliński, P. A., Schulz, R., Kaliaguine, S. and Van Neste, A., Structural transformations of alumina by high energy ball milling. *J. Mater. Res.*, 1993, **8**(11), 2985–2992.
2. Hench, L. L., Bioceramics: from concept to clinic. *J. Am. Ceram. Soc.*, 1991, **74**, 1487–1510.
3. Travitzky, N., Kumar, P., Sandhage, K. H., Janssen, R. and Claussen, N., Rapid synthesis of Al_2O_3 reinforced Fe–Cr–Ni composites. *Mater. Sci. Eng. A*, 2003, **1/2**(344), 245–252.
4. Ganguly, P. and Poole, Warren J., In situ measurement of reinforcement stress in an aluminium–alumina metal matrix composite under compressive loading. *Mater. Sci. Eng. A*, 2003, **352**(1/2), 46–54.
5. Martínez Flores, E., Negrete, J. and Torres Villaseñor, G., Structure and properties of Zn–Al–Cu alloy reinforced with alumina particles. *Mater. Des.*, 2003, **24**(3), 281–286.
6. Wang, Y., Milosevic, O., Gomez, L., Rabanal, M. E., Torralba, J. M., Yang, B. and Towsend, P. D., Thermoluminescence responses from europium doped gadolinium oxide. *J. Phys.: Condens. Matter*, 2006, **18**, 9257–9272.
7. Wang, Wei-Ning, Lenggoro, Wuled I., Terashi, Yoshitake, Kim, Tae Oh and Okuyama, Kikuo, One-step synthesis of titanium oxide nanoparticles by spray pyrolysis of organic precursors. *Mater. Sci. Eng. B*, 2005, **123**(3), 194–202.
8. López Ibáñez, R., Ramos Barrado, J. R., Martín, F., Brucker, F. and Leinen, D., Oxide barrier coatings on steel strip by spray pyrolysis. *Surf. Coat. Technol.*, 2004, **188/189**, 675–683.
9. Castañeda, L., Alonso, J. C., Ortiz, A., Andrade, E., Saniger, J. M. and Bañuelos, J. G., Spray pyrolysis deposition and characterization of titanium oxide thin films. *Mater. Chem. Phys.*, 2003, **77**(3), 938–944.
10. Takehisa Fukui, Satoshi Ohara, Makio Naito *et al.*, Performance and stability of SOFC anode fabricated from NIO-YSZ composite particles. *J. Power Sources*, 2002, **110**(1), 91–95.
11. Vallet-Regí, M., Rodríguez-Lorenzo, L. M., Ragel, C. V., Salinas, A. J. and González-Calbet, J. M., Control of structural type and particle size in alumina synthesized by the spray pyrolysis method. *Solid State Ionics*, 1997, **101–103**, 197–203.
12. Vallet-Regí, M., Ragel, V., Román, J., Martínez, J. L., Labeau, M. and González-Calbet, J. M., Texture evolution of SnO_2 synthesized by pyrolysis of an aerosol. *J. Mater. Res.*, 1993, **8**(1), 138–144.
13. Pacewska, B. and Keshr, M., Thermal transformations of aluminium nitrate hydrate. *Thermochim. Acta*, 2002, **385**(1/2), 73–80.
14. Lang, R. L., Ultrasonic atomization of liquids. *J. Acoust. Soc. Am.*, 1962, **34**(1), 6–8.
15. Liu, T.-Q., Sakurai, O., Mizutani, N. and Kato, M., *J. Mater. Sci.*, 1986, **21**, 3698.
16. *Software of Philips Analytical X-Ray*. Philips Electronics N.V. 1996–1999.
17. *Pcpdfwin Program, Version 1.1—September 1995*.
18. Morniroli, J. P., Vankieken, D. and Winter, L., *Electron Diffraction Pattern Simulations for Windows Program*.
19. Paglia, G., *Determination of the structure of γ-alumina using empirical and first principles calculations combined with supporting experiments*. Doctoral Thesis. Curtin University of Technology, February 2004.
20. Zhou, R. S. and Snyder, R. L., Structures and transformations mechanisms of the η, γ and θ transition aluminas. *Acta Crystallogr.*, 1991, **B47**, 617–630.
21. Lippens, B. C. and de Boer, J. H., Study of phase transformations during calcination of aluminum hydroxides by selected area electron diffraction. *Acta Crystallogr.*, 1964, **17**, 1312–1321.
22. Welton-Holzer, J., McCarthy, G., North Dakota State University, Fargo, North Dakota, USA, ICDD Grant-in-Aid, 1989 (in *JCPDS-ICDD Copyright 1993*).
23. Peter Østbo, N., *Evolution of alpha phase alumina in agglomerates upon addition to cryolitic melts*. Doctoral Thesis. Norwegian University of Science and Technology, May 2002.

24. Tok, A. I. Y., Boey, F. Y. C. and Zhao, X. L., Novel synthesis of Al_2O_3 nano-particles by flame spray pyrolisis. *J. Mater. Process. Technol.*, 2006, **178**, 270–273.
25. Li, J., Pan, Y., Xiang, C., Ge, Q. and Guo, J., Low temperature synthesis of ultrafine α-Al_2O_3 powder by a simple aqueous sol–gel process. *Ceram. Int.*, 2006, **32**(5), 587–591.
26. Levin, I., Bendersky, I. A., Brandon, D. G. and Rühle, M., Cubic to monoclinic phase transformations in alumina. *Acta Mater.*, 1997, **45**(9), 3659–3669.
27. Levin, I. and Brandon, D., Metastable alumina polymorphs: crystal structures and transition sequences. *J. Am. Ceram. Soc.*, 1998, **81**(8), 1995–2012.
28. Wefer, K. and Misra, C., *Alcoa Technical Paper No. 19*. Alcoa Laboratories 1987.
29. Webster, T. J., Hellenmeyer, E. L. and Price, R. L., Increased osteoblast functions on theta + delta nanofiber alumina. *Biomaterials*, 2005, **26**, 953–960.